Nanostructured Ternary Nanocomposite of rGO/CNTs/MnO₂ for High-Rate Supercapacitors

Hao Jiang, Yihui Dai, Yanjie Hu, Weina Chen, and Chunzhong Li*

Key Laboratory for Ultrafine Materials of Ministry of Education, School of Materials Science and Engineering, East China University of Science and Technology, 130 Meilong Road, Shanghai 200237, China

S Supporting Information

ABSTRACT: A three-dimensional (3D) nanostructure comprised of ternary rGO/CNTs/MnO₂ nanocomposites was successfully developed and prepared for high-rate supercapacitors. The optimized nanocomposite exhibited a high specific capacitance (SC) of 319 F g^{-1} with enhanced rate capability (222 F g^{-1} even at 60 A g^{-1}) and cycling stability (85.4% retention of original capacity after cycling for 3000 times) in a 1 M Na₂SO₄ aqueous solution. Such outstanding capacitive behaviors are mainly attributed to smart nanostructures, which possess several advantages as supercapacitor electrodes, such as easy access pseudoactive species with high utilization and fast ion/electron transfer and also a strong interaction between the 3D rGO/CNTs carbon matrix and pseudoactive MnO₂ nanoflakes. It is concluded that the present 3D rGO/CNTs/MnO₂ nanocomposites can serve as promising electrode materials for advanced supercapacitors.

KEYWORDS: Reduced graphene oxide, Carbon nanotubes, MnO₂, Nanocomposite, Supercapacitor
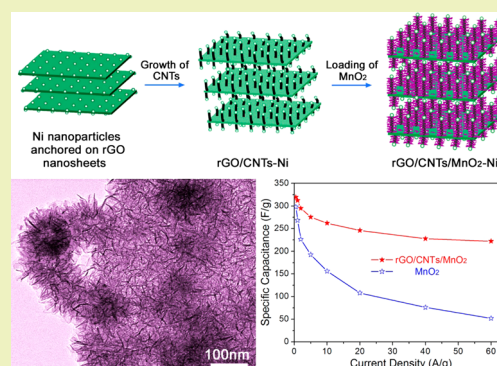
■ INTRODUCTION

For the past few years, considerable research efforts have been focused on high-power and energy-density storage devices due to the ever-increasing needs for high-power applications such as electric vehicles, hybrid electric vehicles, and other power supply facilities.[1−5] Supercapacitors have attracted intense interest owing to their combining merits, i.e., high power density of conventional dielectric capacitors and high energy density of batteries.[4,6] On the basis of the energy storage mechanism, supercapacitors can be divided into electrical double-layer capacitors (EDLCs) and pseudocapacitors, basically, the former use carbon-active materials as electrodes and the latter use redox-active materials. The key to develop supercapacitors is the design and synthesis of high-performance electrode materials. Among the various materials studied so far, MnO₂ has been considered as the most promising candidate in view of its low cost, environmentally friendly nature, and especially its high theoretical capacity.[7−9] More significantly, MnO₂-based nanomaterials are usually applied in neutral aqueous electrolytes, which can meet the current environmental requirements of "green electrolytes" in supercapacitors. However, the intrinsic poor conductivity of MnO₂ (10^{-5} to 10^{-6} S cm^{-1})[10] leads to an unsatisfying charge−discharge rate performance, especially for high-power devices.

To solve the problem, one strategy is to combine the two kinds of electrode materials by coupling MnO₂ with EDLCs-based carbon materials considering their high power density and long cycling life.[4,11,12] Graphene, a rapidly rising star, has been the focus of world attention in energy storage fields owing to its ultrahigh surface area, outstanding electrical conductivity,

and strong mechanical stability.[13] Some reports show that the combination of metal oxide-based electrode materials with graphene can greatly improve the electrochemical performance.[14−16] For instance, Yan et al.[14] used surface carbon as the reducing agent to prepare graphene/MnO₂ composite electrodes with the aid of necessary binder and conducting agents, which delivered a specific capacitance of 310 F/g at a scan rate of 2 mV/s. Chen et al.[17] reported the integration of GO and needle-like MnO₂ crystals, which endowed the composites with better electrochemical behaviors for supercapacitors. It is widely known that the surface area of graphene highly depends on the number of graphene layers. However, a critical challenge in the fabrication and application of graphene is to weaken the strong van der Waals force of the π-stacked layers in graphite.
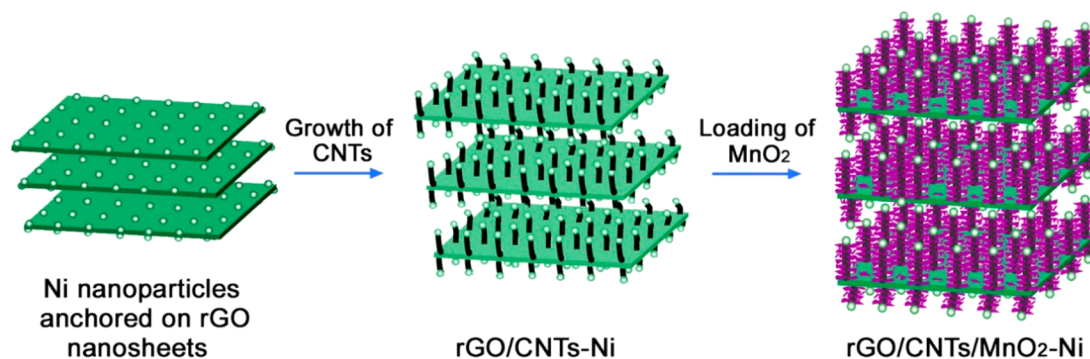
In this work, we demonstrated the synthesis of ternary rGO/CNTs/MnO₂ nanocomposites, in which CNTs were grown in between the rGO nanosheets layers by a chemical vapor deposition forming intriguing three-dimensional (3D) nanostructures, and then MnO₂ nanoflakes were loaded on the 3D rGO/CNTs framework. In this architecture, CNTs were used as "stabilizers" or "spacers" between graphene layers forming a 3D conductive network and, hence, avoiding the aggregation of graphene and accelerating electron transportation. Meanwhile, the as-designed nanostructures can also create amounts of

Scheme 1. Schematic Illustration of Experimental Steps for Preparation of 3D rGO/CNTs/MnO$_2$ Nanocomposites

Ni nanoparticles anchored on rGO nanosheets — Growth of CNTs → rGO/CNTs-Ni — Loading of MnO$_2$ → rGO/CNTs/MnO$_2$-Ni

porous configurations, which may further shorten the diffusion path of ions. The resulting nanocomposites, when applied as supercapacitor electrodes, exhibited high specific capacitance with outstanding rate capability and high cycling stability.

EXPERIMENTAL SECTION

General. All the reagents used in the experiment were of analytical grade (Sigma-Aldrich) and were used as received.

Method. *Synthesis of rGO/CNTs-Ni.* Graphene oxide (GO) was prepared from natural graphite flake (Alfa Aesar) via the modified Hummers method, which was described elsewhere.[14] In a typical procedure, 54 mg of GO was well dispersed in 108 mL of deionized (DI) water by sonication for 30 min. Afterward, an appropriate amount of nickel nitrate was slowly added into the suspension, followed by few drops of diluted ammonia solution, and then stirred for 2 h at room temperature. The obtained precursor, i.e., GO-Ni(OH)$_2$ composite was collected by freeze-drying and was annealed at 500 °C for 2 h in flowing argon to obtain rGO-Ni. Then the CVD method was used to grow CNTs on the Ni-loaded rGO sheets at 650 °C for 15 min with acetylene as the carbon source based on our previous work.

Synthesis of rGO/CNTs/MnO$_2$. Typically, 30 mg rGO/CNTs-Ni was first dispersed in 30 mL deionized water. Then an appropriate 0.1 M KMnO$_4$ solution was slowly added into the suspension, and the mixed solution was transferred to a 50 mL Teflon-lined stainless steel autoclave. The autoclave was sealed tightly and subjected to an elevated temperature of 150 °C in air oven for 6 h and then naturally cooled. The precipitate was collected by filtration, washed several times with DI water and absolute ethanol, and finally dried at 60 °C overnight for further characterizations.

Characterizations. The as-prepared products were characterized with X-ray powder diffractometer (XRD; Rigaku D/max 2550VB/PC with Cu Kα radiation (40 kV, 100 mA)), scanning electron microscopy (FESEM; Hitachi S-4800, 15 kV), and transmission electron microscopy (TEM; JEOL 2010, 200 kV) operated at 200 kV equipped with an energy dispersive X-ray spectrometer (EDS). N$_2$ adsorption/desorption was carried out by Brunauer−Emmett−Teller (BET) measurements using a Micromertics 2010 analyzer. Thermogravimetric analysis (TGA, Q500) was proceeded with a heating rate of 10 °C min^{-1} under flowing nitrogen.

Electrochemical Measurements. Electrochemical measurements (Autolab PGSTAT30 potentiostat) were conducted in a 1 M Na$_2$SO$_4$ aqueous solution using a three-electrode mode. The working electrode was prepared as follows. The active material powder (80 wt %), acetylene black (15 wt %), and polyvinylidene fluoride (PVDF, 5 wt %) were first mixed in NMP, and then an appropriate absolute ethanol was added into the mixture to promote homogeneity. After that, the mixture was coated onto the graphite paper (1 cm^2) to form the electrode layer by drying at 120 °C for around 2 h. The mass loading of active materials is about 0.8 mg cm^{-2}. The reference and counter electrodes were Ag/AgCl electrode and platinum foil, respectively. Typical CV curves were measured between −0.2 and 0.8 V.

RESULTS AND DISSUSION

The experimental steps for the resulting nanocomposites are illustrated in Scheme 1. The detailed process for the preparation of rGO/CNTs/MnO$_2$ are listed in the Experimental Section. The XRD pattern of the as-obtained rGO/CNTs/MnO$_2$ nanocomposites with ∼75.6 wt % MnO$_2$ (TG curve, Figure S3, Supporting Information) is shown in Figure 1.
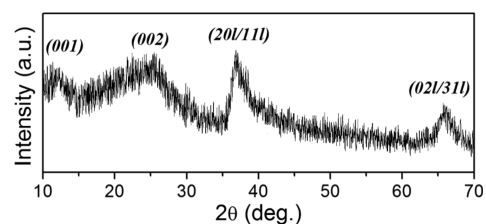

Figure 1. XRD pattern of the rGO/CNTs/MnO$_2$ nanocomposites.

All of the diffraction peaks correspond to monoclinic K-birnessite MnO$_2$ (JCPDS no. 80-1098), which consists of 2D nanosheets of edge-shared MnO$_6$ octahedral separated from each other with K$^+$ ions and water molecules located at the interlayer space. No other characteristic peaks from the impurities are detected in the spectrum. The first two peaks are indexed to (001) and (002) basal reflections, while two other peaks arise from the (20l/11l) and (02l/31l) diffraction bands, respectively.[18,19]

Figure 2a shows the corresponding SEM image of the composites. It is noted that CNTs are well distributed on the surface of rGO nanosheets, and MnO$_2$ nanoflakes are well grown on the surface of the whole rGO/CNTs framework. A high-magnification SEM image is also provided in Figure S1 (Supporting Information). The detailed structure of the rGO/CNTs/MnO$_2$ nanocomposites was further examined by TEM, as shown in Figure 2(b−d). Figure 2b exhibits that the CNTs grown from the CVD method are multi-walled CNTs. Notably, most of the Ni nanoparticle catalysts disappear at the top of CNTs. A TEM image of Ni nanoparticles loaded rGO is provided in Figure S2 (Supporting Information). The tip growth mechanism of CNTs in this work has been discussed elsewhere.[20] From the observation of a high-magnification TEM image, an obvious hole at the top of the CNTs can be observed, labeled by a yellow dotted circle in Figure 2c. The addition of acid KMnO$_4$ with strong oxidizing ability is responsible for the dissolution of Ni nanoparticles. In addition, it is clear that the MnO$_2$ nanoflakes are well grown on the CNT wall and the surface of rGO, which coincide exactly with the observation of SEM. By controlling the KMnO$_4$ concentration,
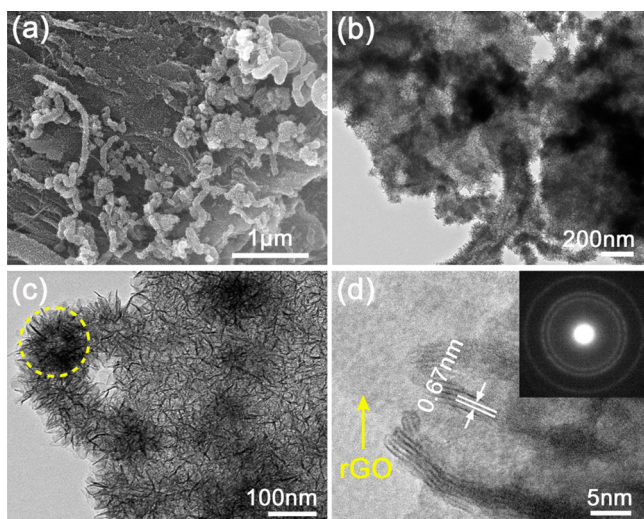
71

dx.doi.org/10.1021/sc400313y | ACS Sustainable Chem. Eng. 2014, 2, 70−74

Figure 2. (a) SEM image. (b) Low-magnification and (c) high-magnification TEM images. (d) High-resolution TEM images of the rGO/CNTs/MnO$_2$ nanocomposites. Inset shows the corresponding SAED pattern.

the thickness of the MnO$_2$ layer can be easily varied. As shown in Figure 2d, the interplanar distance of the MnO$_2$ nanoflake is measured to be 0.67 nm,[19] which is in accordance with the literature for birnessite-type MnO$_2$. The electron diffraction (ED) pattern (Figure 2d, inset), taken from a randomly chosen area, shows a polycrystalline nature.

The rGO/CNTs/MnO$_2$ nanocomposites also show a high BET surface area of 140 m^2 g^{-1} with a pore volume of 0.36 m^3 g^{-1}. The N$_2$ adsorption and desorption isotherms and pore size distribution are shown in Figure 3. A distinct hysteresis loop is
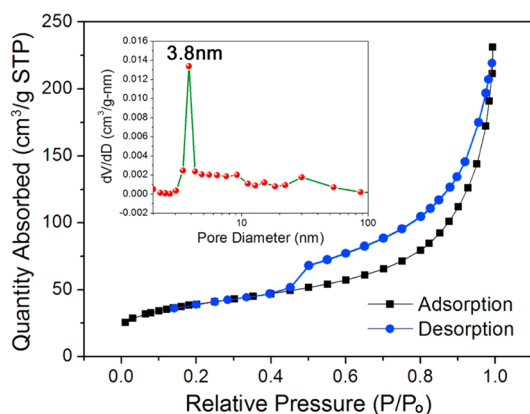

Figure 3. N$_2$ adsorption/desorption isotherms and pore size distribution curves (inset) of the rGO/CNTs/MnO$_2$ nanocomposites.

noticed in the larger range of 0.45−1.0 P/P$_0$, suggesting the presence of mesoporous and macroporous structures.[9] The pore size distribution was estimated to have an average diameter of 3.8 nm calculated from the desorption data using the BJH model. The high BET surface area and porous feature of the rGO/CNTs/MnO$_2$ make it possible that electrons and ions transport easily and efficiently in the electrode matrix, thus leading to better electrochemical performances.

Figure 4a shows the CV curves of the as-synthesized rGO/CNTs/MnO$_2$, rGO/CNTs, and pure MnO, at a scan rate of 20 mV s^{-1} in a 1 M Na$_2$SO$_4$ aqueous solution. All the samples

present a typical capacitive behavior with rectangular and symmetric CV curves. It is noted that the specific capacitance of the rGO/CNTs/MnO$_2$ nanocomposites is just above pure MnO$_2$ but much higher than rGO/CNTs. In the CV curves, an obvious gradient angle appears from −0.2 to 0 V and from 0.6 to 0.8 V for pure MnO$_2$, while an almost vertical line can be observed for rGO/CNTs/MnO$_2$, indicating that the electrical conductivity of the rGO/CNTs/MnO$_2$ has been greatly improved, suggesting an excellent power performance. This also demonstrates the strong synergistic effect of the electric double layer-/pseudo-capacitive contributions from the rGO/CNTs framework and MnO$_2$ nanoflakes, respectively. To obtain a better understanding of the effect of MnO$_2$ content on the electrochemical performance of the nanocomposites, the specific capacitances based on different MnO$_2$ contents are provided in Figure S4 of the Supporting Information according to their CV measurements. The results indicated that the rGO/CNTs/MnO$_2$ nanocomposites with 75.6% MnO$_2$ content possessed the highest specific capacitance. To further investigate the electrochemical performance of the optimized rGP/CNTs/MnO$_2$ nanocomposites, the galvanostatic charge−discharge curves of the rGO/CNTs/MnO$_2$ nanocomposites were measured from 0.5 to 20 A g^{-1}, as shown in Figure 4b. It is shown that the charging curves are basically symmetrical to their discharging counterparts, suggesting good electrochemical behavior. A maximum specific capacitance of 319 F g^{-1} can be achieved at a low current density of 0.5 A g^{-1}. Figure 4c further illustrates the relationship between specific capacitance and current density. The data of pure MnO$_2$ is also provided as a comparison. It is found that the capacitance retention of rGO/CNTs/MnO$_2$ is much better than pure MnO$_2$ with an increase in current density. A specific capacitance of 222 F g^{-1} is maintained for rGO/CNTs/MnO$_2$, while only 52 F g^{-1} for pure MnO$_2$ at a very high current density of 60 F g^{-1}. Ragone plots are also presented in Figure 4d for rGO/CNTs/MnO$_2$, pure MnO$_2$, and rGO/CNTs. The energy densities can be estimated to be 44.3 Wh kg^{1-} for rGO/CNTs/MnO$_2$, 41.4 Wh kg^{1-} for pure MnO$_2$, and 18.1 Wh kg^{1-} for rGO/CNTs at a power density of 250 W kg^{-1}. More importantly, the energy density still maintains a high value of 30.8 Wh kg^{1-} for rGO/CNTs/MnO$_2$, while only 7.2 Wh kg^{1-} and 6.7 Wh kg^{1-} are retained for pure MnO$_2$ and rGO/CNTs, respectively, even when the power density is as high as 30000 W kg^{-1}. The capacitive performances of the rGO/CNTs/MnO$_2$ nanocomposites are encouraging, which is of great potential as the electrode materials for high-rate charge−discharge applications in supercapacitors.

The long-term cycling stability of the rGO/CNTs/MnO$_2$ nanocomposites is also studied by CV measurement at a scan rate of 50 mV s^{-1} for 3000 cycles, as depicted in Figure 5. The as-designed nanocomposites exhibited a high electrochemical stability that still kept about 85.4% capacitance retention after cycling for 3000 times. The high cycling stability can be mainly due to the synergistic effects among rGO, CNTs, and MnO$_2$. It is noted that the electrolyte gradually turns a light shade of brown after the cycling test, indicating partial dissolution of MnO$_2$ into electrolyte, which would probably be the reason of the capacitance decrease.

On the basis of the above discussions, the capacitive performance of the rGO/CNTs/MnO$_2$ nanocomposites is better than the reported pure MnO$_2$ nanostructures, even with more intriguing morphologies, such as ultrafine MnO$_2$ nanowires,[21] 3D claw-like MnO$_2$ nanostructures.[22] In a
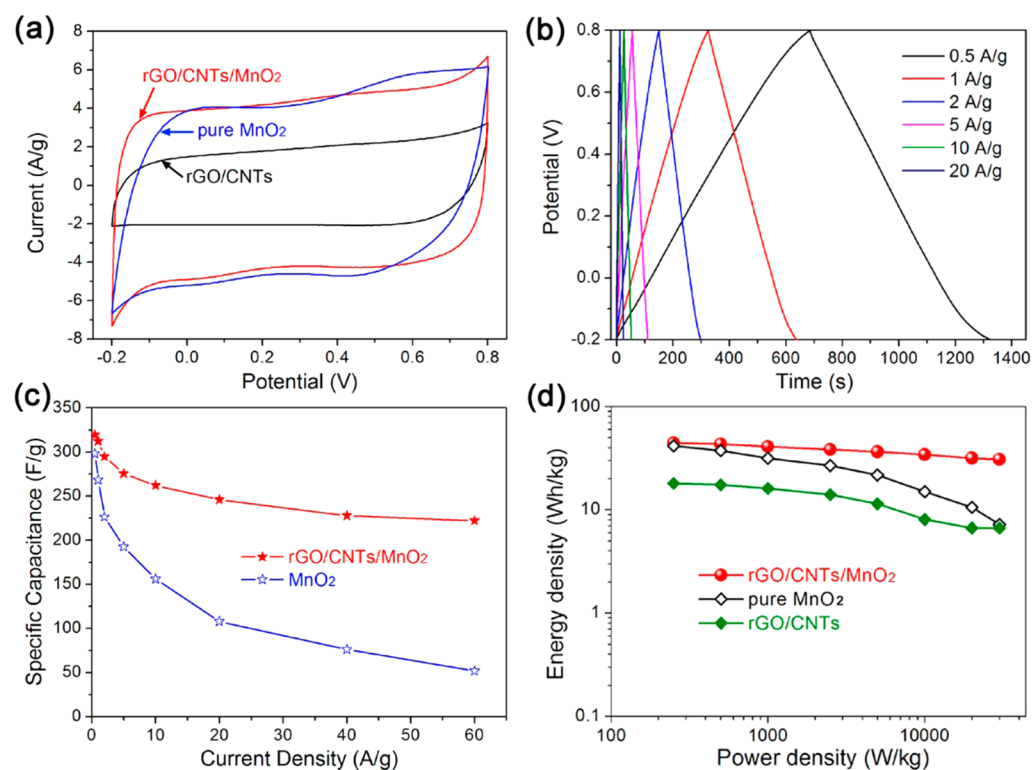
Figure 4. (a) CV curves of the rGO/CNTs/MnO$_2$, pure MnO$_2$, and rGO/CNTs at a scan rate of 20 mV s^{-1}, respectively. (b) Charge−discharge curves of the rGO/CNTs/MnO$_2$ at current densities of 0.5−20 A g^{-1}. (c) Specific capacitance as a function of different current densities of rGO/CNTs/MnO$_2$ and pure MnO$_2$. (d) Ragone plots of rGO/CNTs/MnO$_2$, pure MnO$_2$, and rGO/CNTs.
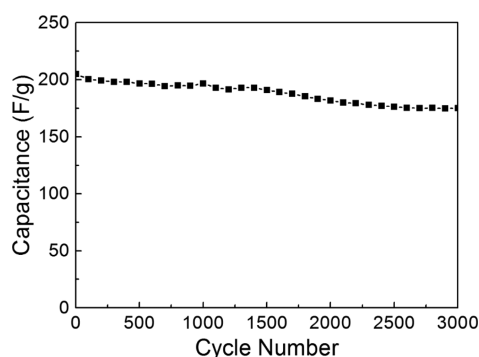

Figure 5. Specific capacitance versus cycling number at 50 mV s^{-1} of the rGO/CNTs/MnO$_2$ nanocomposites.

previous report, MnO$_2$ multilayer nanosheets clusters were synthesized by Feng et al.,[23] which showed a high specific capacitance of 521 F g^{-1} at 5 mV s^{-1} but only 42 F g^{-1} at 50 mV s^{-1} (205 F g^{-1} for this work, Supporting Information). Compared with most of the reported MnO$_2$-based nanocomposites, our as-designed material also exhibited superior electrochemical performance, such as MnO$_2$/multi-walled CNTs composites,[24] MnO$_2$ nanosheets/graphene nanocomposites,[25] ultrafine β-MnO$_2$/polypyrrole nanorod composites,[26] Zn$_2$SnO$_4$/MnO$_2$ core/shell nanocable-carbon microfiber hybrids,[27] MnO$_2$/activated carbon textiles,[28] and so forth. Recently, Lee et al.[29] reported MnO$_2$ nanoparticles enriched in poly(3,4-ethylenedioxythiophene) nanowires, showing a high specific capacitance of 250 F g^{-1} at 5 mA cm^{-2}. However, these materials systems showed a poor stability, 10% capacity loss after 500 cycles (only 3.9% capacity loss for our work). Several advantages are supposed to account for the intriguing

electrochemical performances of the as-obtained 3D rGO/CNTs/MnO$_2$ nanocomposites. First, the construction of the rGO/CNTs framework is conducive to greatly enhancing the electrical conductivity of MnO$_2$ by forming a highly conductive network, which will ensure the high rate capability of electrode materials. Second, MnO$_2$ nanoflakes have been well grown and well dispersed all over the 3D rGO/CNTs framework, constructing amounts of porous configuration. The porous feature leads to more contact area with the electrolyte and can also accommodate the possible volume change during cycling. Therefore, high specific capacitance and cycling stability were obtained. Third, an obvious synergistic effect was achieved between high power density electric double-layer capacitance material (rGO/CNTs) and high energy density pseudocapacitance material (MnO$_2$). It is therefore reckoned to be a promising candidate for supercapacitors.

■ CONCLUSION

In summary, we demonstrated the design and synthesis of 3D rGO/CNTs/MnO$_2$ nanocomposites for high-performance supercapacitor applications. The optimized nanocomposite exhibited a high specific capacitance of 319 F g^{-1} with enhanced rate capability (222 F g^{-1} even at 60 A g^{-1}) and cycling stability (85.4% retention of original capacity after cycling for 3000 times) in a 1 M Na$_2$SO$_4$ aqueous solution. Such excellent electrochemical behaviors are mainly attributed to the smart nanostructures, which can provide fast ion and electron transfer by forming a 3D conductive network, superior reversible redox reactions of the pseudoactive materials, efficient utilization of the highly accessible MnO$_2$ species, and a strong interaction between the rGO/CNTs carbon matrix and pseudoactive MnO$_2$ nanoflakes. The present findings are

important not only for the synthesis of 3D rGO/CNTs/MnO$_2$ nanocomposites but also for the development of advanced electrode materials with better electrochemical performance, which may provide huge potential for applications in supercapacitors.

■ ASSOCIATED CONTENT

Ⓢ Supporting Information

Additional supporting figures. This material is available free of charge via the Internet at http://pubs.acs.org.

■ AUTHOR INFORMATION

Corresponding Author

*Tel.: +86-21-64252055. Fax: +86-21-64250624. E-mail: czli@ecust.edu.cn.

Notes

The authors declare no competing financial interest.

■ ACKNOWLEDGMENTS

■ REFERENCES

(1) Simon, P.; Gogotsi, Y. Materials for electrochemical capacitors. *Nat. Mater.* **2008**, *7*, 845−854.

(2) Lee, S. W.; Yabuuchi, N.; Gallant, B. M.; Chen, S.; Kim, B. S.; Hammond, P. T.; Shao-Horn, Y. High-power lithium batteries from functionalized carbon-nanotube electrodes. *Nat. Nanotechnol.* **2010**, *5*, 531−537.

(3) Guo, S. J.; Dong, S. J. Graphene nanosheets: synthesis, molecular engineering, thin film, hybrids, and energy and analytical applications. *Chem. Soc. Rev.* **2011**, *40*, 2644−2672.

(4) Jiang, H.; Ma, J.; Li, C. Z. Mesoporous carbon incorporated metal oxide nanomaterials as supercapacitor electrodes. *Adv. Mater.* **2012**, *24*, 4197−4202.

(5) Yan, J.; Sumboja, A.; Khoo, E.; Lee, P. S. V$_2$O$_5$ loaded on SnO$_2$ nanowires for high-rate Li ion batteries. *Adv. Mater.* **2010**, *23*, 746−750.

(6) Jiang, H.; Lee, P. S.; Li, C. Z. 3D Carbon based nanostructures for advanced supercapacitors. *Energy Environ. Sci.* **2013**, *6*, 41−53.

(7) Wei, W. F.; Cui, X. W.; Chen, W. X.; Ivey, D. G. Manganese oxide-based materials as electrochemical supercapacitor electrodes. *Chem. Soc. Rev.* **2011**, *40*, 1697−1721.

(8) Kim, J. H.; Lee, K. H.; Overzet, L. J.; Lee, G. S. Synthesis and electrochemical properties of spin-capable carbon nanotubes sheet/MnO$_x$ composites for high-performance energy storage devices. *Nano Lett.* **2011**, *11*, 2611.

(9) Jiang, H.; Yang, L. P.; Li, C. Z.; Yan, C. Y.; Lee, P. S.; Ma, J. High-rate electrochemical capacitors from highly graphitic carbon-tipped manganese oxide/mesoporous carbon/manganese oxide hybrid nanowires. *Energy Environ. Sci.* **2011**, *4*, 1813−1819.

(10) Lang, X. Y.; Hirata, A.; Fujita, T.; Chen, M. W. Nanoporous metal/oxide hybrid electrodes for electrochemical supercapacitors. *Nat. Nanotechnol.* **2011**, *6*, 232−236.

(11) Liu, R.; Duay, J.; Lee, S. B. Heterogeneous nanostructured electrode materials for electrochemical energy storage. *Chem. Commun.* **2011**, *47*, 1384−1404.

(12) Zhang, H.; Cao, G. P.; Wang, Z. Y.; Yang, Y. S.; Shi, Z. J.; Gu, Z. N. Growth of manganese oxide nanoflowers on vertically-aligned carbon nanotube arrays for high-rate electrochemical capacitive energy storage. *Nano Lett.* **2008**, *8*, 2664−2668.

(13) Singh, V.; Joung, D.; Zhai, L.; Das, S.; Khondaker, S. I.; Seal, S. Graphene based materials: Past, present and future. *Prog. Mater. Sci.* **2011**, *56*, 1178−1271.

(14) Yan, J.; Fan, Z. J.; Wei, T.; Qian, W. Z.; Zhang, M. L.; Wei, F. Fast and reversible surface redox reaction of graphene−MnO$_2$ composite as supercapacitor electrode. *Carbon* **2010**, *48*, 3825−3833.

(15) Ghosh, D.; Giri, S.; Das, C. K. Preparation of CTAB-assisted hexagonal platelet Co(OH)$_2$/graphene hybrid composite as efficient supercapacitor electrode material. *ACS Sustainable Chem. Eng.* **2013**, *1* (9), 1135−1142.

(16) Pumera, M. Graphene-based nanomaterials for energy storage. *Energy Environ. Sci.* **2011**, *4*, 668−674.

(17) Chen, S.; Zhu, J. W.; Wu, X. D.; Han, Q. F.; Wang, X. Graphene oxide−MnO$_2$ nanocomposites for supercapacitors. *ACS Nano* **2010**, *4*, 2822−2830.

(18) Jiang, H.; Li, C. Z.; Sun, T.; Ma, J. A green and high energy density asymmetric supercapacitor based on ultrathin MnO$_2$ nanostructures and functional mesoporous carbon nanotube electrodes. *Nanoscale* **2012**, *4*, 807−812.

(19) Xia, H.; Lai, M.; Lu, L. Nanoflaky MnO$_2$/carbon nanotube nanocomposites as anode materials for lithium-ion batteries. *J. Mater. Chem.* **2010**, *20*, 6896−6902.

(20) Fan, Z. J.; Yan, J.; Zhi, L. J.; Zhang, Q.; Wei, T.; Feng, J.; Zhang, M. L.; Qiang, W. Z.; Wei, F. A three-dimensional carbon nanotube/graphene sandwich and its application as electrode in supercapacitors. *Adv. Mater.* **2010**, *22*, 3723−3728.

(21) Jiang, H.; Zhao, T.; Ma, J.; Yan, C. Y.; Li, C. Z. Ultrafine manganese dioxide nanowire network for high-performance supercapacitors. *Chem. Commun.* **2011**, *47*, 1264−1266.

(22) Yu, P.; Zhang, X.; Wang, D. L.; Wang, L.; Ma, Y. W. Shape-controlled synthesis of 3D hierarchical MnO$_2$ nanostructures for electrochemical supercapacitors. *Cryst. Growth Des.* **2009**, *9*, 528−533.

(23) Feng, Z. P.; Li, G. R.; Zhong, J. H.; Wang, Z. L.; Ou, Y. N.; Tong, Y. X. MnO$_2$ multilayer nanosheet clusters evolved from monolayer nanosheets and their predominant electrochemical properties. *Electrochem. Commun.* **2009**, *11*, 706−710.

(24) Jiang, R. R.; Huang, T.; Tang, Y.; Liu, J. L.; Xue, L. G.; Zhuang, J. H.; Yu, A. S. Factors influencing MnO$_2$/multi-walled carbon nanotubes composite's electrochemical performance as supercapacitor electrode. *Electrochim. Acta* **2009**, *54*, 7173−7179.

(25) Li, Z. P.; Wang, J. Q.; Liu, X. H.; Liu, S.; Ou, J. F.; Yang, S. G. Electrostatic layer-by-layer self-assembly multilayer films based on graphene and manganese dioxides sheets as novel electrode materials for supercapacitors. *J. Mater. Chem.* **2011**, *21*, 3397−3403.

(26) Zang, J. F.; Li, X. D. In situ synthesis of ultrafine beta-MnO2/polypyrrole nanorod composites for high-performance supercapacitors. *J. Mater. Chem.* **2011**, *21*, 10965−10969.

(27) Bao, L. H.; Zang, J. F.; Li, X. D. Flexible Zn$_2$SnO$_4$/MnO$_2$ core/shell nanocable-carbon microfiber hybrid composites for high-performance supercapacitor electrodes. *Nano Lett.* **2011**, *11*, 1215−1220.

(28) Bao, L. H.; Li, X. D. Towards textile energy storage from cotton T-shirts. *Adv. Mater.* **2012**, *24*, 3246−3252.

(29) Liu, R.; Duay, J.; Lee, S. B. Redox exchange induced MnO$_2$ nanoparticle enrichment in poly(3,4-ethylenedioxythiophene) nanowires for electrochemical energy storage. *ACS Nano* **2010**, *4*, 4299−4307.

74

dx.doi.org/10.1021/sc400313y | *ACS Sustainable Chem. Eng.* 2014, 2, 70−74